Quartz Crystal Microbalance Technique for analysis of Cooling Crystallization

ARTICLE *in* ANALYTICAL CHEMISTRY · JANUARY 2013

Impact Factor: 5.64

1 AUTHOR:

Li-Shang Liu

6 PUBLICATIONS **287** CITATIONS

SEE PROFILE

analytical chemistry

Article

pubs.acs.org/ac

Quartz Crystal Microbalance Technique for Analysis of Cooling Crystallization

Li-Shang Liu,[†] JongMin Kim,[‡] Sang-Mok Chang,[‡] Guang Jin Choi,[§] and Woo-Sik Kim*[,†]

[†]Department of Chemical Engineering, Kyung Hee University, Yongin-si, Gyeonggi-do, 446-701, Korea

[‡]Department of Chemical Engineering, Dong-A University, Hadan 840, Saha, Busan 604-741, Korea

[§]Department of Pharmaceutical Engineering, Soon Chun Hyang University, 8 Asan, Chungnam 336-745, Korea

Supporting Information

ABSTRACT: A quartz crystal microbalance (QCM) technique is developed for the in situ analysis of the cooling crystallization processes of crystal nucleation and growth. In contrast to conventional techniques based on property changes in the solid or solution phase, the proposed QCM technique simultaneously exploits property changes in both the solid and solution phases, such as the solid mass and liquid viscosity, to analyze the crystallization processes. When initially cooling the solution, an increase in the solution viscosity is reflected in the QCM responses for the resonant frequency and resonant resistance. With further cooling, the resonant frequency and resonant resistance sharply change at the induction point of crystal nucleation, as the viscous liquid film on the sensor suddenly shifts to an elastic solid phase. Thereafter, the QCM responses are mainly controlled by the suspension viscosity due to simultaneous crystal nucleation and growth with further cooling. As a result, the QCM responses allow accurate measurement of the induction point and metastable zone width during the cooling crystallization. Additional mechanistic information on the crystallization, including molecular cluster formation, crystal nucleation, and crystal growth, is also extracted from a resonant frequency−resistance plot (F−R plot) of the QCM responses when varying the cooling conditions.

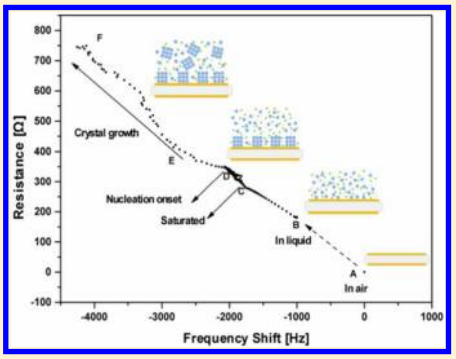

Due to its significant advantages, facilitating process design and operation, cooling crystallization is important for the single crystal preparation of proteins and organic chemicals in biology and crystallography and for the separation and purification of fine chemicals, pharmaceuticals, petrochemicals, and food additives in the chemical industry.[1] Thus, the key phenomena of cooling crystallization, including crystal nucleation, growth, and the metastable zone width, have already been extensively investigated due to their determining roles in the crystal size, distribution, habits, purity, and polymorphs.

According to most previous studies, two kinds of method have generally been adopted to analyze crystal nucleation, detecting the physical property changes in the liquid phase related with crystal nucleation or direct detection of the crystal appearance.[2] In the first case, the detection methods typically depend on changes in the density, electrical conductivity, ultrasound velocity, turbidity, absorption spectra, refraction index, and thermal analysis of the liquid phase during crystal nucleation.[3] For example, when using attenuated total reflection Fourier transform infrared (ATR-FTIR) spectroscopy, a sudden drop in the solute concentration is detected at the crystal nucleation onset point.[4] The turbidity of a solution has also been used to determine the induction point of crystal nucleation.[5] However, noise can easily affect the accuracy of this type of measurement. Thus, Bernardes and da Piedade adopted a thermal analysis technique to analyze crystal nucleation based on the heat of the crystallization.[6] Yet, the crystallization energy involved in crystal nucleation is really small, making it barely possible to pinpoint the induction point of crystal nucleation. The dielectric constant of a solution has also been exploited to sense the onset of crystal nucleation. Similarly, this property change during crystal nucleation is too weak to determine the exact induction point of crystal nucleation.[7]

Meanwhile, in the case of the direct detection of solid crystals, focused beam reflectance measurements (FBRM) based on laser beam scattering have been frequently used to determine the induction point of nucleation. According to Fujiwara's study, FBRM outperformed ATR-FTIR and naked-eye methods in terms of accuracy and sensitivity for measuring the induction point of nucleation.[8] This result is reasonable when considering Mullin's study that found an absence of significant changes in the solution properties even after the crystal nuclei grew to a detectable size, indicating a much longer time-lag for solution property changes than for solid property changes.[9] Boskey and Posner also demonstrated the accuracy of detecting the induction point of nucleation using the changes in the solid phase over the changes in the solution phase in the reaction crystallization of hydroxyapatite.[10] Notwithstanding,

Received: February 24, 2013
Accepted: April 3, 2013
Published: April 3, 2013

most of the above-mentioned methods only provide limited information on the onset point of crystal nucleation during crystallization.

Over the last 2 decades, quartz crystal microbalances (QCMs), an electro-acoustic technique, have been widely applied to measure property changes in gases, liquids, and solids. In a study by Sun et al, a QCM was used to measure low humidity based on modifying the quartz sensor surface with polypyrrol.[11] Plus, Ji et al. showed that a QCM could selectively detect aromatic gases when using sensors modified by grapheme and ionic liquid films.[12] QCMs have also been used for recognizing the stereoisomers of mandelic acid on a molecular level in both the gas[13] and liquid phases,[14] sensing DNA hybridization[15] and a cancer marker in the liquid phase,[16] investigating the multideposition mechanism of the metal organic framework of HKUST-1,[17] and monitoring the gelation of cellulose[18] and conformational changes of proteins[19] and polymers.[20] Furthermore, due to the versatility, reliability, and sensitivity for in situ sensing small variations in the working environment around a quartz crystal sensor, QCM techniques have already been applied to detect electrical deposition, solution pH changes, film phase transitions, bacteria detection and quantification, and cell growth mechanisms.[21]

Consequently, on the basis of a supersensitivity to mass change (1.07 ng/Hz), a QCM method could be reasonably expected to provide an accurate analysis of crystal nuclei formation on a molecular level. In addition, online detection now offers improved supersaturation control strategies during crystallization to produce the desired crystal shape, purity, structure, and size.[22] Accordingly, the present study presents a QCM technique for analyzing the cooling crystallization phenomena of crystal nucleation and growth that exploits the unique ability of a QCM for simultaneously detecting property changes in both the liquid and solid phases. While cooling the solution for crystallization, the QCM responses are used to monitor the resonant frequency and resonant resistance. Plus, the cooling rate is varied to infer mechanistic information on the supersaturation accumulation, crystal nucleation, and growth from the QCM responses, while also measuring the induction point of crystal nucleation and the metastable zone width. The accuracy and reliability of the QCM method are validated on the basis of a comparison with FBRM measurements.

EXPERIMENTAL SECTION

The 4-amino-*N*-(4-methylpyrimidin-2-yl)benzenesulfonamide, also known as sulfamerazine, was purchased from Sigma-Aldrich with a 99%+ purity. The acetonitrile was supplied by Daejung Co. (purity 99.5%), and the quartz crystal sensors (frequency of 9 MHz) were supplied by Princeton Applied Research. The gold electrode on the quartz crystal sensor was cleaned with a piranha solution (H_2SO_4:H_2O_2 = 3:1 v/v) and DI water, dried with a nitrogen flow to remove any contamination, and then fixed with a lead wire using an electrically conductive adhesive at 150 °C for 2 h. Then, the gold electrode was characterized by using a contact angle analyzer (Surface Electro Optics Co.) and cyclic voltammetry (CH Instruments). As shown in the Supporting Information (Figure S-1), the contact angle of the gold electrode, 72 ± 1 °C, well matches those of other studies.[23] Also, the reduction and oxidation peaks of cyclic voltammogram revealed the clean gold of the electrode (Supporting Information, Figure S-2).[24]

Thereafter, the quartz crystal sensors were used for the QCM measurements without further sensor surface modifications.

The cooling crystallization of sulfamerazine was conducted in a 300 mL batch crystallizer with gentle agitation of 300 rpm, as shown in Figure 1. Here, the sulfamerazine solution of 20 g/L

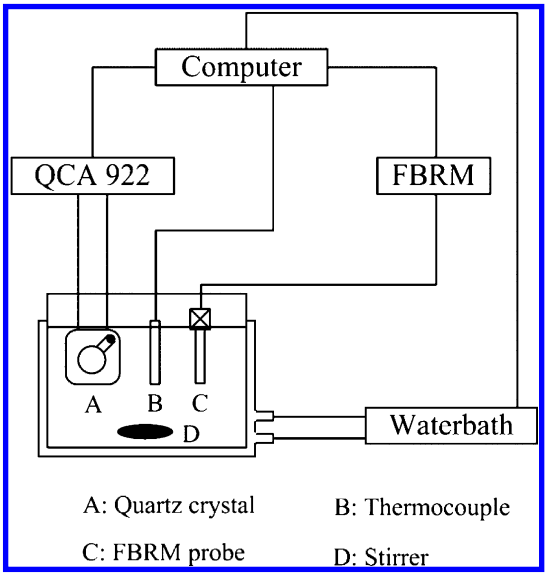

Figure 1. Block diagram of cooling crystallization experimental system.

was prepared by dissolving the sulfamerazine in an acetonitrile/water solvent mixture (80%/20% v/v) that was degassed by ultrasound. Once in the crystallizer, the sulfamerazine solution was initially heated to 45 °C and then cooled to 24 °C at a constant cooling rate. The cooling rate was varied at 0.3, 0.5, 0.7, and 0.9 °C/min. Blank control experiments using a blank solution with no solute were also carried out under the same conditions in order to compare the QCM responses from the solute solution. The QCM responses for the resonant frequency and resonant resistance were monitored during the cooling crystallization using an oscillation detector (QCA 922, Seiko EG&G). Here, the same quartz crystal sensor was used in all the experiments to ensure consistent piezoelectric sensor responses. During the cooling crystallization, the gold sensor surface was analyzed by using a tabletop scanning electron microscope (Hitachi TM-1000). Simultaneously, the cooling crystallization was also monitored by using FBRM measurements to validate the accuracy and reliability of the QCM measurements.

QCM THEORY AND PRINCIPLES

Basic Relationship. A QCM sensor is composed of a piece of AT cut quartz crystal plated with two metal electrodes. Due to the piezoelectricity under an alternating current, the quartz crystal vibrates in a thickness shear mode (TSM), and an acoustic wave propagates perpendicular to the crystal surface. Without any disturbance, the quartz vibrates infinitely at a basic frequency. However, when the oscillation is disturbed by an adsorbed material, the oscillation wave propagation from the QCM surface varies with the properties of the adsorbed material. The frequency of the shear wave of the oscillating quartz crystal, called the resonant frequency, is linearly correlated with the rigid mass loading on the quartz surface, as described by Sauerbrey's equation for the idealized mode:[25]

dx.doi.org/10.1021/ac400585c | *Anal. Chem.* 2013, 85, 4790−4796

$$\Delta f_m = \frac{-2f_0^2}{A\sqrt{\mu_q \rho_q}}\Delta m \quad (1)$$

where Δf_m is the resonant frequency shift due to the loaded mass on the sensor Δm, f_0 is the fundamental frequency of the resonator (9 MHz), A is the active area of the quartz crystal, called the electrode surface (0.2 cm^2), ρ_q is the density of the quartz crystal (2.648 g/cm^2), and μ_q is its shear modulus (2.947×10^{11} dyn/cm^2).

In addition, the resonant frequency shift depends on the physical property of the liquid phase on the sensor surface. According to Kanazawa and Gordon, the resonant frequency shift in a solution can be described as follows[26]

$$\Delta f_l = -f_0^{3/2}\sqrt{\frac{\rho_L \eta_L}{\pi \mu_q \rho_q}} \quad (2)$$

where η_L is the dynamic viscosity of the solution and ρ_L is the density of the solution. From eqs 1 and 2, it is evident that variations in the solid mass and liquid viscosity cause a resonant frequency shift of the sensor for the liquid-phase QCM measurement.[27]

In the electrical equivalent circuit of the oscillating quartz crystal shown in Figure 2a, the resonant resistance R_1 reflects

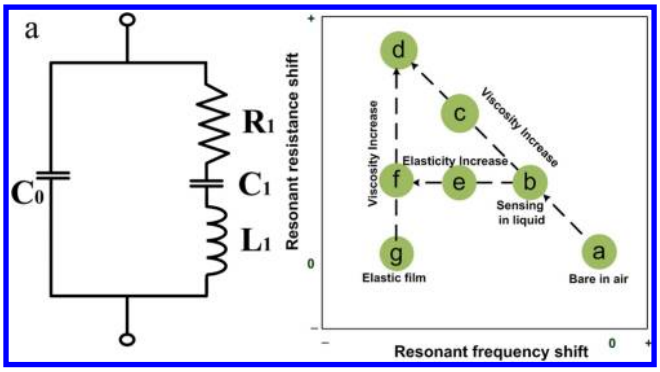

Figure 2. (a) Electrical equivalent circuit of quartz crystal sensor and (b) explanation of interface viscosity and elasticity variation patterns using the $F-R$ model.

the degree of mechanical vibration energy loss due to damping in a viscous liquid, as described below[28]

$$R_1 = \frac{A\sqrt{2\pi f_0 \rho_L \eta_L}}{\kappa^2} \quad (3)$$

where κ is the electromechanic coupling factor of the quartz resonator. According to eq 3, the resonant resistance shift depends on the physical properties of the liquid, such as the viscosity and density.

Using the equivalent circuit, the basic resonant frequency of the quartz crystal can be estimated from $f_0 = 1/2\pi(C_1L_1)^{1/2}$, where the capacitance C_1 reflects the elasticity, while the inductance L_1 reflects the mass of the quartz crystal. Therefore, using the above eqs 1−3, the property changes in both the solid and liquid phases, including the mass, viscosity, and elasticity, can be estimated via the resonance frequency and resonant resistance shifts of the QCM.

***F−R* Diagram Model.** If the QCM responses on a time scale are converted to a plot of the resonant resistance according to the resonant frequency ($F-R$ diagram), this can provide information on both the property changes and the phase shift of the solute during the crystallization. As described in Figure 2b, point "a" is the QCM response in the original state of the undisturbed bare sensor in air, and the shift from point "a" to point "b" results from the response change of the QCM when it is immersed in the liquid phase. Thus, the shifting path b → c → d, an extension of a → b, indicates an increase in the viscosity of the liquid film without an elasticity change. Here, the viscous penetration of the liquid film increases as the liquid viscosity increases. Thus, the response shift in path b → e → f is due to an increase in the elasticity of the film. In this pathway, the resonant frequency is markedly reduced without a significant change in the resonant resistance, as there is no serious vibration energy loss. This shift occurs when the mass synchronously vibrates with the sensor, i.e., in the case of a rigid mass. Therefore, the $\Delta F-\Delta R$ model can be used to infer the phase changes in the film adsorbed on the sensor surface. Further details of the $\Delta F-\Delta R$ model can be found in previous reports.[27−29]

RESULTS AND DISCUSSION

QCM Responses to Cooling Crystallization. The QCM responses of the resonant frequency (F) and resonant resistance (R) for the cooling crystallization of sulfamerazine are shown in Figure 3 (curves I and II using dots). Before time

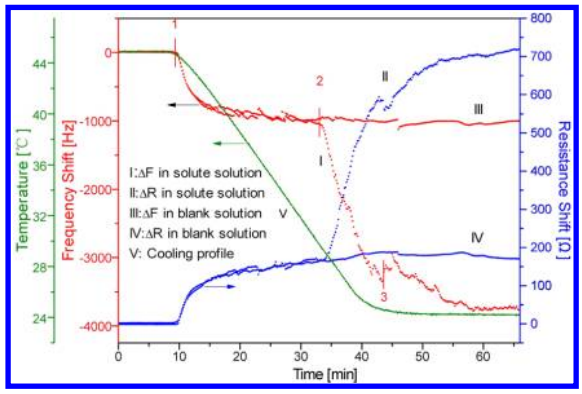

Figure 3. In situ resonant responses of QCM during cooling of solute solution (20 g/L of sulfamerazine) and blank solution (pure solvent) at a cooling rate of 0.7 °C/min. (I) resonant frequency shift during cooling of solute solution. (II) resonant resistance shift during cooling of solute solution. (III) resonant frequency shift during cooling of blank solution. (IV) resonant resistance shift during cooling of blank solution. (V) cooling profile of solution.

t_1, while the sulfamerazine (SMZ) solution (20 g/L) was maintained at a constant temperature of 45 °C, the resonant frequency and resonant resistance remained stable due to an invariant environment on the sensor. However, when the SMZ solution was cooled at a constant cooling rate of 0.7 °C/min (from time t_1 to t_3), the resonant frequency and resonant resistance varied due to changes in the solution viscosity. When decreasing the temperature, the solution viscosity increased, causing a more viscous vibration energy loss on the sensor. Therefore, decreasing the temperature resulted in a reduction of the resonance frequency and an increase in the resonant resistance, as depicted in eqs 2 and 3. It is interesting to note that the QCM response profiles for the resonant frequency and resonant resistance were markedly deflected at time t_2, probably due to the induction of crystal nucleation on the sensor at time t_2. That is, the formation of crystals at t_2 likely caused the

dx.doi.org/10.1021/ac400585c | Anal. Chem. 2013, 85, 4790−4796

increase in the viscosity and mass loading on the sensor, resulting in the sudden changes of the resonant frequency and resonant resistance. Crystal formation at t_2 was visually confirmed, as the clear SMZ solution suddenly became a turbid suspension at t_2 (Supporting Information, Figure S-3). Microscopic images also revealed crystal formation on the sensor surface at t_2. As shown in Figure 4a, there were no

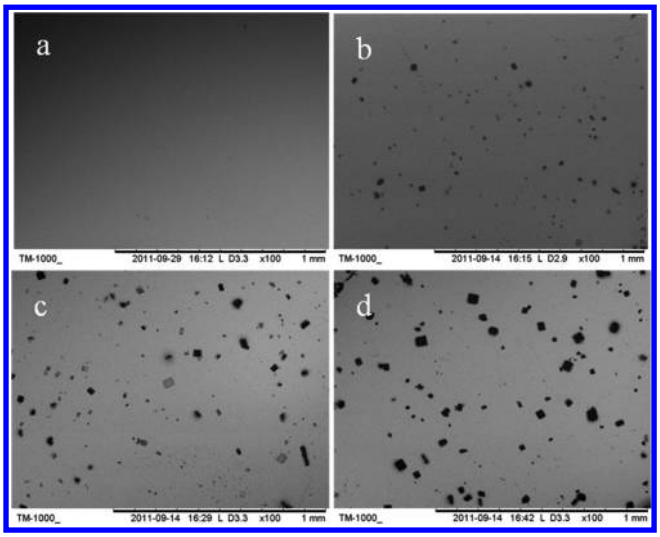

Figure 4. SEM photographs of QCM sensor surface conditions during cooling of solute solution (20 g/L of sulfamerazine, 0.7 °C/min cooling rate): (a) before point 2 (nucleation induction), (b) right after point 2, (c) 3 min after point 2, and (d) 6 min after point 2.

crystals on the sensor surface before t_2. However, right after t_2, several small crystals were found on the sensor (Figure 4b), and the population and size of the crystals then increased as the solution was cooled further (Figure 4c,d). Therefore, these results established that the first crystal nucleation was induced at time t_2 (induction point of crystal nucleation) during the cooling crystallization.

It should be mentioned that the viscosity of the liquid is almost linearly changed within a moderate range of temperature (T), resulting in the resonant response (Δf and R) proportional to $T^{1/2}$, according to eqs 2 and 3. When using an immerging QCM cell to detect the viscosity change of the liquid phase, one electrode is opened to the liquid phase and the other electrode is exposed to the air phase trapped in the closed cell structure to eliminate the influence of liquid damping on the oscillation. So, the temperature change in the liquid phase is spontaneously reflected in the electrode responses in the liquid phase, whereas the electrode responses in the air phase lags much behind the temperature change in the liquid phase due to the high thermal resistance of the cell wall and air. Therefore, two such different environments of liquid and air phases to the electrodes in the immerging QCM cell result in the deviation of the QCM resonant responses from their proportionality to $T^{1/2}$, as decreasing the temperature.

This deviation of the resonant responses in the cooling crystallization was confirmed by the measurement of QCM resonant response in the blank solution. A solute-free solution (blank solution) was cooled at the same cooling rate of 0.7 °C/min (curves III and IV in Figure 3). The QCM responses of the resonant frequency and resonant resistance for the blank solution were coincident with those of the SMZ solution before time t_2. However, no sudden changes in the resonant frequency and resonant resistance occurred, even with further cooling of the blank solution, due to the lack of crystal nucleation. Therefore, these results support that the sudden changes of the QCM responses in the SMZ solution originated from the induction of crystal nucleation.

After the induction point, the crystal nucleation and growth continued simultaneously on the basis of the supersaturation. Thus, the resonant frequency and resonant resistance continued to vary significantly until reaching a setting temperature (t_3), at which point both became relatively stable, although some fluctuation still occurred due to the collision, adhesion, and detachment of bulk crystals on the sensor surface resulting from the suspension agitation.

The cooling crystallization of sulfamerazine was also monitored by FBRM, where the detection method was based on the beam reflection by the particles/crystals in the suspension. As shown in Figure 5 (curve III), the FBRM

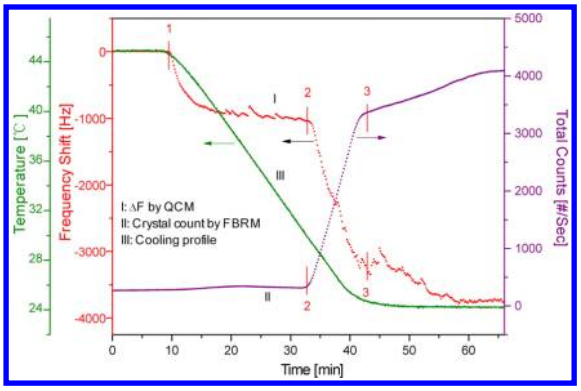

Figure 5. Comparison of QCM monitoring of cooling crystallization (20 g/L sulfamerazine concentration, 0.7 °C/min cooling rate) with FBRM monitoring under the same crystallization conditions: (I) resonant frequency shift of QCM, (II) crystal numbers in solution counted by FBRM, (III) cooling profile of solution.

showed no signal change up to time t_2 (induction point). However, after time t_2, the crystal population increased rapidly due to spontaneous crystal nucleation. Thus, the induction point of crystal nucleation matched exactly with that detected by the QCM. Here, it should be noted that since the particle counting of FBRM was based on the light beam reflection by the particle in the suspension, there might occur a slight reflection even in the clear solution. In addition, the air bubble in the liquid brought on by the mechanical agitation might cause the slight reflection of the light beam, misidentifying the particle numbers. Thus, it might be a reason why a small number of particles was misdetected by the FBRM in the clear solution before the crystal nucleation.

***F*–*R* Diagram Analysis.** The resonant frequency and resonant resistance on a time scale (F–t and R–t plots in Figure 3) were converted to a resonant frequency vs resonant resistance plot (F–R diagram), as shown in Figure 6. When the air environment around the quartz crystal sensor was changed to a liquid environment (SMZ solution), the QCM response in the F–R diagram shifted from A → B due to the sudden increased viscosity and density of the liquid, similar to the response shift a → b in the model plot (Figure 2b). The response shifting path B → C in the cooling crystallization then slightly deviated from the ideal path (extended line of dashed arrows) due to the inherent piezoelectric property of the quartz

dx.doi.org/10.1021/ac400585c | Anal. Chem. 2013, 85, 4790–4796

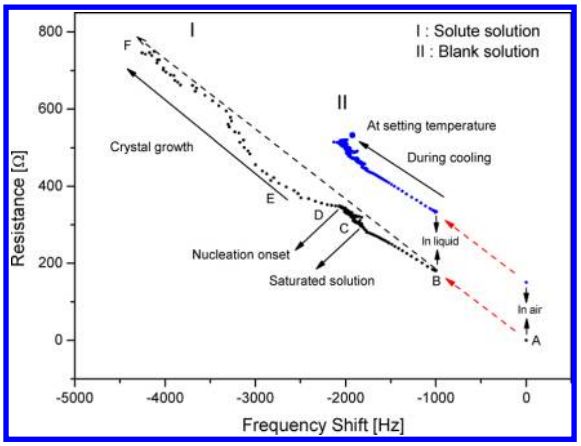

Figure 6. *F*−*R* plot of QCM responses. The dashed line indicates the direction of pure liquid viscosity change (QCM response from air phase to liquid phase): (I) QCM responses during cooling of solute solution (20 g/L sulfamerazine concentration, 0.7 °C/min cooling rate) and (II) QCM responses during cooling of the blank solution (pure solvent, 0.7 °C/min cooling rate).

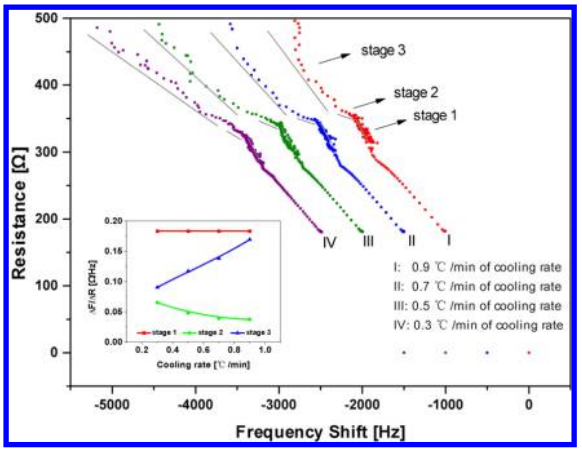

Figure 7. *F*−*R* plot of QCM responses during cooling crystallization of sulfamerazine at various cooling rates (20 g/L sulfamerazine concentration): (I) at a cooling rate of 0.9 °C/min, (II) at a cooling rate of 0.7 °C/min, (III) at a cooling rate of 0.5 °C/min, and (IV) at a cooling rate of 0.3 °C/min. (Inset) Slope change of *F*−*R* plot at each stage during cooling crystallization depending on cooling rate: ■, slope at stage 1; ●, slope at stage 2; and ▲, slope at stage 3.

sensor depending on the temperature. When comparing the QCM responses on a time scale (*F*−*t* and *R*−*t* plots in Figure 3), point C in the *F*−*R* diagram was found to correspond to when the SMZ solution was saturated. When further cooling the solution, the solution became supersaturated, resulting in the response shift from C → D due to the increased degree of supersaturation. Here, it is interesting to note that the shifting path C → D was parallel to the ideal path (dashed arrows), indicating an ideal viscous behavior of the supersaturated solution. The thickness of the liquid layer vibrating with the sensor also increased as the degree of supersaturation increased, thereby causing the response shift from C to D. Crystal nucleation was initially induced at point D, and the QCM response shifted almost horizontally to E, similar to the ideal elastic response b → e → f in the model plot (Figure 2b), due to a slight change in the resonant resistance relative to the significant drop in the resonant frequency during this period. According to nucleation theory, solute molecules are assembled into clusters in a supersaturated solution and then suddenly turn into solid crystals once they grow above a critical size. Therefore, the present results would seem to infer that the molecular clusters in the supersaturated solution were reconstructed as an elastic solid by the crystal nucleation process. During this short restructuring period (about 10 s), the decrease in the resonant frequency was mainly due to a rigid mass loading of crystals on the sensor. An increment of viscous friction by the nuclei may have contributed to the slight increase in the resonant resistance. Thereafter, the *F*−*R* response of E → F was predominantly determined by the increased viscoelasticity of the suspension due to spontaneous crystal growth during the crystallization.

Meanwhile, since there were no solute molecules in the blank solution to generate supersaturation and crystal nucleation, the QCM response monotonically followed a shifting path that depended purely on the viscosity change when cooling the blank solution. Thus, when reaching the setting temperature, the QCM response converged to a final point.

Figure 7 shows more details on the influence of the cooling rate on the crystallization. On the basis of the QCM response explained in the *F*−*R* representation, the cooling crystallization was characterized by three stages: stage 1 for accumulating supersaturation, stage 2 for inducing crystal nucleation, and stage 3 for crystal growth. During stage 1, since the QCM response was predominantly dictated by the viscosity change of the supersaturated solution, the response shifting path was independent of the cooling rate. Thus, the vibrational energy loss per unit mass ($\Delta R/\Delta F$ values in *F*−*R* diagram) remained constant at 0.183 Ω/Hz (inset figure). However, during stage 2 inducing crystal nucleation, the response shifting path varied with the cooling rate, as the induction point depended on the supersaturation level. At a high cooling rate of 0.9 °C/min, the first crystal nucleation was induced at a high supersaturation level. In this case, the viscous clusters were quickly restructured into huge numbers of elastic solids (nuclei) on the sensor, resulting in a low $\Delta R/\Delta F$ of 0.037 Ω/Hz in the *F*−*R* diagram. However, when reducing the cooling rate to 0.3 °C/min, the crystal nucleation was induced at a lower supersaturation level. In this case, the restructuring of the viscous clusters into elastic solids was much slower and resulted in a smaller population. Plus, due to the longer nucleation period, the growth of nuclei on the sensor also occurred simultaneously, thereby increasing the vibrational friction of the sensor and producing a marked increase in $\Delta R/\Delta F$ to 0.065 Ω/Hz. During stage 3, the QCM response predominantly reflected the crystal growth dependent on the cooling rate. Due to the high nucleation with a high cooling rate of 0.9 °C/min, this produced a high $\Delta R/\Delta F$ of 0.17 Ω/Hz. However, this was reduced to 0.08 Ω/Hz when decreasing the cooling rate to 0.3 °C/min.

Metastable Zone Width. Using the QCM responses to the cooling crystallization of sulfamerazine, the metastable zone width (MSZW), the temperature gap between the saturation and nucleation points, was estimated with various cooling rates (Figure 8). When increasing the cooling rate, the crystal nucleation was induced at a higher critical supersaturation (lower temperature), resulting in a wider MSZW, yet shorter induction time. Thus, a MSZW of 7.8 °C and induction time of 27 min when using a cooling rate of 0.3 °C/min changed to a MSZW of 10.5 °C and induction time of 10 min when using a cooling rate of 1.1 °C/min. These results for the MSZW and induction time agreed well with the FBRM measurements within an error range.

dx.doi.org/10.1021/ac400585c | *Anal. Chem.* 2013, 85, 4790−4796

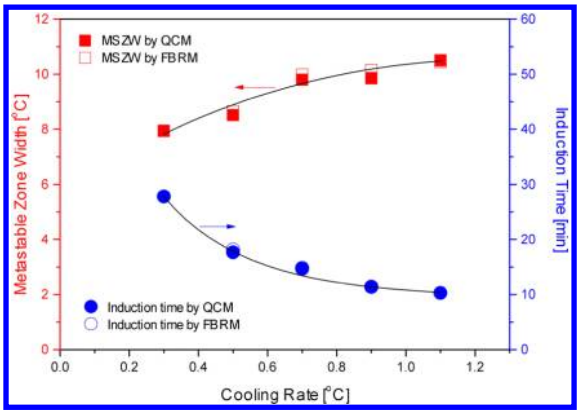

Figure 8. Comparison of metastable zone width and induction time for cooling crystallization of sulfamerazine (20 g/L) measured by QCM and FBRM: ■, MSZW measured by QCM; □, MSZW measured by FBRM; ●, induction time measured by QCM; and ○, induction time measured by FBRM.

CONCLUSIONS

A QCM technique was shown to be applicable to analyze cooling crystallization. During the cooling crystallization of sulfamerazine, the vibrational frequency (F) and resistance (R) of the quartz crystal sensor clearly responded to property changes in the solution on the sensor. That is, when cooling the solution, the viscous friction of the solution on the sensor increased, thereby decreasing the resonant frequency (F) and increasing the resonant resistance. However, at the induction of crystal nucleation with further cooling, the resonant frequency and resonant resistance changed rapidly due to the increased viscosity and mass loading on the sensor. Thereafter, the QCM responses varied gradually following the crystal growth with the cooling temperature.

An F−R diagram of the QCM responses identified three clear stages of interfacial property changes on the sensor: supersaturation accumulation, crystal nucleation, and crystal growth. During the first stage, the viscous friction of the liquid film on the sensor increased when decreasing the temperature. Thus, the F−R response at this stage followed the ideal viscous change. During the second stage, the viscous responses suddenly shifted to elastic responses, indicating that the viscous liquid film on the sensor had suddenly changed into an elastic solid due to crystal nucleation. During the third and final stage, crystal nucleation and growth occurred simultaneously in the suspension, which increased the viscoelasticity in the suspension. Thus, the resonant response at this stage belonged to a middle range between the pure viscous and elastic responses.

The QCM resonant frequency and resonant resistance responses allowed easy estimation of the induction point of nucleation and metastable zone width, both of which were highly reproducible and accurate when compared with FBRM measurements.

ASSOCIATED CONTENT

Supporting Information

Figures S-1−S-3. This material is available free of charge via the Internet at http://pubs.acs.org.

AUTHOR INFORMATION

Corresponding Author

*Tel: +82 31 201 2970. Fax: +82 31 273 2971. E-mail: wskim@khu.ac.kr.

Notes

The authors declare no competing financial interest.

ACKNOWLEDGMENTS

This work was supported by a Mid-Career Researcher through an NRF grant funded by MEST (2010-0017993).

REFERENCES

(1) Astier, J. P.; Veesler, S. *Cryst. Growth Des.* **2008**, *8*, 4215−4219.
(2) Simon, L. L.; Nagy, Z. K.; Hungerbuhler, K. *Chem. Eng. Sci.* **2009**, *64*, 3344−3351.
(3) Marciniak, B. *J. Cryst. Growth* **2002**, *236*, 347−356.
(4) Bakhbakhi, Y.; Charpentier, P.; Rohani, S. *Can. J. Chem. Eng.* **2005**, *83*, 267−273.
(5) Rabesiaka, M.; Porte, C.; Bonnin-Paris, J.; Havet, J. L. *J. Cryst. Growth* **2011**, *332*, 75−80.
(6) Bernardes, C. E. S.; da Piedade, M. E. M. *J. Therm. Anal. Calorim.* **2010**, *100*, 493−500.
(7) He, G. W.; Tjahjono, M.; Chow, P. S.; Tan, R. B. H.; Garland, M. *Org. Process Res. Dev.* **2010**, *14*, 1477−1480.
(8) Fujiwara, M.; Chow, P. S.; Ma, D. L.; Braatz, R. D. *Cryst. Growth Des.* **2002**, *2*, 363−370.
(9) Mullin, J. W. *Crystallization*, 4th ed.; Butterworth-Heinemann: Oxford, 2001.
(10) Söhnel, O.; Garside, J. *Precipitation: Basic Principles and Industrial Applications*; Butterworth-Heinemann: New York, 1992.
(11) Sun, Y. L.; Wu, R. J.; Huang, Y. C.; Su, P. G.; Chavali, M.; Chen, Y. Z.; Lin, C. C. *Talanta* **2007**, *73*, 857−861.
(12) Ji, Q. M.; Honma, I.; Paek, S. M.; Akada, M.; Hill, J. P.; Vinu, A.; Ariga, K. *Angew. Chem. Int. Ed.* **2010**, *49*, 9737−9739.
(13) Guo, H. S.; Kim, J. M.; Kim, S. J.; Chang, S. M.; Kim, W. S. *Langmuir* **2009**, *25*, 648−652. Guo, H. S.; Kim, J. M.; Chang, S. M.; Kim, W. S. *J. Nanosci. Nanotechnol.* **2009**, *9*, 2937−43.
(14) Kim, J. M.; Chang, S. M.; Li, F.; Guo, H. S.; Kim, W. S. *J. Nanosci. Nanotechnol.* **2011**, *11*, 7676−7681.
(15) Nie, L. B.; Yang, Y.; Li, S.; He, N. Y. *Nanotechnology* **2007**, *18*, 305501. Nie, L. B.; Chen, Z.; Zou, H. J.; Chang, H. *J. Nanosci. Nanotechnol.* **2013**, *13*, 2077−2080. Nie, L. B.; Yang, Y.; Li, S.; Wang, J. Q.; Hou, Q. L. *J. Nanosci. Nanotechnol.* **2007**, *7*, 2927−2929.
(16) Wang, D. Z.; Tang, W.; Wu, X. J.; Wang, X. Y.; Chen, G. J.; Chen, Q.; Li, N.; Liu, F. *Anal. Chem.* **2012**, *84*, 7008−7014.
(17) Stavila, V.; Volponi, J.; Katzenmeyer, A. M.; Dixon, M. C.; Allendorf, M. D. *Chem. Sci.* **2012**, *3*, 1531−1540.
(18) Verissimo, M. I. S.; Pais, A. A. C. C.; Gomes, M. T. S. R. *Carbohydr. Polym.* **2010**, *82*, 363−369.
(19) Peh, W. Y. X.; Reimhult, E.; Teh, H. F.; Thomsen, J. S.; Su, X. D. *Biophys. J.* **2007**, *92*, 4415−4423.
(20) Zhang, G. Z. *Macromolecules* **2004**, *37*, 6553−6557.
(21) Cooper, M. A.; Singleton, V. T. *J. Mol. Recognit.* **2007**, *20*, 154−184. Mirmohseni, A.; Hassanzadeh, V. *J. Appl. Polym. Sci.* **2001**, *79*, 1062−1066. Kusano, H.; Kitagawa, M. *IEICE T Electron* **2008**, *E91c*, 1876−1880. Zhou, T.; Marx, K. A.; Warren, M.; Schulze, H.; Braunhut, S. J. *Biotechnol. Prog.* **2000**, *16*, 268−277. Johnson, K. C. C.; Mendez, F.; Serpe, M. J. *Anal. Chim. Acta* **2012**, *739*, 83−88. Speight, R. E.; Cooper, M. A. *J. Mol. Recognit.* **2012**, *25*, 451−473.
(22) Nagy, Z. K.; Chew, J. W.; Fujiwara, M.; Braatz, R. D. *J. Process Control* **2008**, *18*, 399−407.
(23) Borges, J.; Campina, J. M.; Souza, H. K. S.; Goncalves, M. P.; Silva, A. F. *Soft Matter* **2012**, *8*, 1190−1201.
(24) Park, J. W.; Lee, H.-Y.; Kim, J. M.; Yamasaki, R.; Kanno, T.; Tanaka, H.; Tanaka, H.; Kawai, T. *J. Biosci. Bioeng.* **2004**, *97*, 29−32.
(25) Sauerbrey, G. Z. *Z. Phys.* **1959**, *155*, 206−222.

(26) Kanazawa, K. K.; Gordon, J. G. *Anal. Chim. Acta* **1985**, *175*, 99−105.
(27) Kim, J. M.; Chang, S. M.; Muramatsu, H.; Isao, K. *Korean J. Chem. Eng.* **2011**, *28*, 987−1008.
(28) Muramatsu, H.; Tamiya, E.; Karube, I. *Anal. Chem.* **1988**, *60*, 2142−2146.
(29) Muramatsu, H.; Kim, J. M.; Chang, S. M. *Anal. Bioanal. Chem.* **2002**, *372*, 314−321.